Phase Difference Based RFID Navigation for Medical Applications

Andreas Wille
Institut für Neuroinformatik
Ruhr-Universität Bochum
44780 Bochum, Germany
Email: andreas.wille@ini.rub.de

Magdalena Broll
Institut für Neuroinformatik
Ruhr-Universität Bochum
44780 Bochum, Germany
Email: magdalena.broll@ini.rub.de

Susanne Winter
Institut für Neuroinformatik
Ruhr-Universität Bochum
44780 Bochum, Germany
Email: susanne.winter@ini.rub.de

***Abstract*—RFID localization is a promising new field of work that is eagerly awaited for many different types of applications. For use in a medical context, special requirements and limitations must be taken into account, especially regarding accuracy, reliability and operating range. In this paper we present an experimental setup for a medical navigation system based on RFID. For this we applied a machine learning algorithm, namely support vector regression, to phase difference data gathered from multiple RFID receivers. The performance was tested on six datasets of different shape and placement within the volume spanned by the receivers. In addition, two grid based training sets of different size were considered for the regression. Our results show that it is possible to reach an accuracy of tag localization that is sufficient for some medical applications. Although we could not reach an overall accuracy of less than one millimeter in our experiments so far, the deviation was limited to two millimeters in most cases and the general results indicate that application of RFID localization even to highly critical applications, e. g., for brain surgery, will be possible soon.**

I. Introduction

Medical navigation is used more and more in different surgical fields like neurosurgery, orthopedics, or traumatology [1][2][3]. Navigation systems provide the surgeon with a real-time visualization of his instruments placed in an image dataset or give a visualization of the deviation of his instruments from a preoperatively planned trajectory. The use of these systems can reduce surgical procedures to a minimal area of operation, leading to a better outcome in the sense of less tissue damage and better postoperative recovery.

To demonstrate the relative positions of the patient and medical instruments, both have to be localized by a tracking system. The accuracy of the position estimation of the tracking system is obviously crucial to the success of the surgery. An accuracy of less than 1 mm is required for many applications.

Most state of the art medical tracking systems use optical tracking devices, which detect infrared light emitted or reflected by markers fixed to the patient and the instruments. Although these systems work with a high accuracy, they suffer from severe drawbacks like the size of the reference bases or their dependency on a free line of sight between camera and markers. Another common type of tracking system is based on induction of electricity in markers, which are moved within a magnetic field. In this case the problem of keeping a free line of sight does not occur, but the accuracy is much worse than that of optical systems, because the magnetic field can easily be disturbed by the equipment in the operating room. A more detailed discussion of problems in image-guided surgery can be found, for example, in the work of Peters [4].

As a solution we propose a use of RFID technology to solve the tracking problem in medical navigation and demonstrate its feasibility in this paper. RFID technology allows us to use small and cheap markers, which can even be fixed to medical instruments (as needles or catheters). A prototype for such an application is shown in Fig. 1(a). Furthermore, a direct line of sight onto the markers won't be necessary any longer, so that in the future it could also be possible to track instruments inside the human body. Nevertheless, in our first approach we consider a situation comparable to usual tracking situations in an operating room where a direct line of sight onto the markers is available, meaning that the radio waves do not have to pass through different media on their way from tag to antennas.

So far very few attempts have been made to use RFID equipment for object localization, although this would open a whole new area of applications [5]. One reason for this lack of research is the implicit need of additional measurements, which results in a much more complex hardware setup in comparison to detection tasks. Distance computation based on signal travel times, for example, requires highly precise clocks, while a nearest neighbor strategy with an extensive grid of RFID readers, on the other hand, is quite simple to set up but offers a very limited accuracy, which scales with the distances between the neighboring readers.

A kind of combined approach, however, could overcome these difficulties. For this an easy to observe measurement variable is needed that can be linked to the distance a signal has traveled before reaching a receiver. In previous works the signal strength usually was the indicator of choice but recently Hekemian-Williams et al. showed that phase differences vary more smoothly and are less affected by low signal to noise ratios [6]. By recording multiple phase differences at the same time and interpreting them not directly, but by applying a machine learning algorithm, the need for precise time measurement could be reduced. For our experiments this is realized by a support vector machine, which is known to be a powerful classification and regression algorithm [7]. Thus, in contrast to

978-1-4244-9606-8/11/$26.00 ©2011 IEEE

(a) Experimental tracking catheter of 2 mm diameter equipped with a RFID tag for use in liquid media.

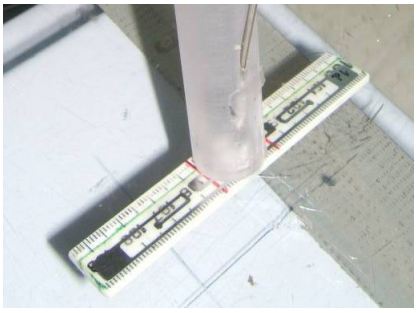

(b) RFID tag used in this work.

Fig. 1. Image of two different RFID tags for medical applications.

nearest neighbor methods, only a few RFID receivers have to be placed within the target area for a precise localization. Of course, this method still needs a time-consuming calibration as the phase difference is used as a nondeterministic indicator (like the received signal strength indication RSSI) and could be disturbed by reflections and varying wavelengths within different media.

The setting of computer guided surgery comes along with several environmental limitations, which help to reduce these problems to a manageable scale. For instance the target area will never be larger than a few cubic meters containing almost no sources of electromagnetic noise. In addition, a reference base can be fixed at the operating table right next to the patient who is in the central area of interest. Thus changes in the environment and their impact on the RFID signal can be monitored easily. And, maybe most important, detailed information about the different media in the target area (i. e., the patient) will usually be available since it is standard procedure to use preoperative images to plan surgery beforehand.

II. Related Work

In the last years several systems for RFID localization have been proposed. Most of them were considered for large scale localization, requiring accuracies of about one meter. The approaches and desired applications, however, differed quite significantly.

For example, Hightower et al. described an indoor location-sensing system (SpotOn), which was based on RSSI and used active RFID tags [8]. Several readers were used to measure the signal strength and a lateration algorithm was used to determine the position of an object. The accuracy depended on the cluster size of the system. Another indoor locating system (LANDMARC) also used active RFID tags but applied the concept of reference tags. It was presented in 2003 by Ni et al., who reported an accuracy of less than 2 m [9].

Ledeczi et al. suggested the radio interferometry method for indoor RF localization and discussed the measurement of phase differences. A special part in this work were the challenges of multipath propagation [10].

In 2009, Zhou and Shi evaluated three localization methods (nearest neighbor, multilateration and support vector machines) for active RFID systems based on RSSI [11]. Regarding the accuracy, the support vector machine (0.31 m) outperformed the other two methods (nearest neighbor: 1.39 m, multilateration: 2.26 m), while the precision results were close to each other.

Hekemian-Williams et al. recently showed that even a localization accuracy of about two millimeters is possible with current RFID equipment when calculating the position estimation based on phase differences [6]. However this work was focused on precise phase difference measurement and not on the overall localization process.

III. Materials and Methods

Medical equipment is subject to strong regulations to ensure the safety of patients. This must be taken into account from the start when developing systems for medical applications and adds significant limitations to the choice of components. Thanks to an industrial cooperation we got access to a prototype of the PRPS tracking system, developed by amedo smart tracking solutions GmbH for medical purposes, which was used to realize the following experiments.

A. Experimental Setup

All experiments for this work were performed inside a plastic basin (50 cm × 90 cm × 20 cm) designed to emulate the human body and head (see Fig. 2) in form and size. There were four antennas (Taoglas PC-29) fixated on each of the longitudinal sides of the basin (in the body and head segment). The placement of the antennas was roughly symmetric but varied slightly in height and longitudinal position. Changes by 90° in orientation were included as well. A drawing of the complete setup is presented in Fig. 3.

During each experiment, a computerized numerical control (CNC) unit with an accuracy of 0.1 mm moved the tag within the basin. In contrast to the position, the orientation of the tag always stayed the same. The type of the tag was Avery AD-222, a standard passive model with a size of 90 mm × 10 mm × 1 mm (see Fig. 1(b)). Each time the tag's movement stopped, an UDL-500 reader beneath the basin triggered the tag and several simultaneous measurements of the phase of the tag's signal at different antennas were taken. These measurements were directly processed by a phase meter included in the PRPS system. By combination of antennas from different sides of the basin, sixteen pairs of antennas with a recorded phase difference each are obtained. All components

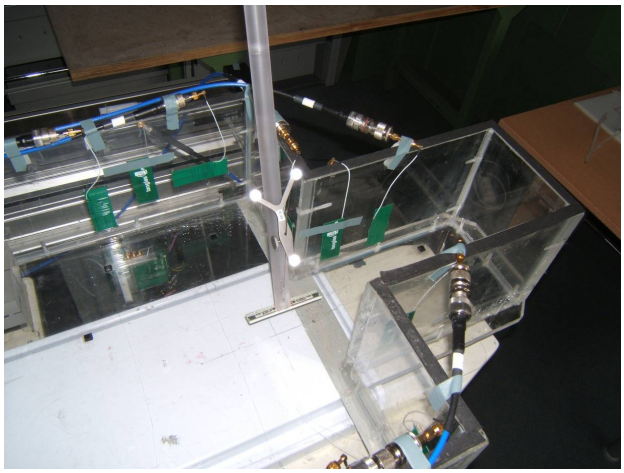

Fig. 2. Experimental setup – Image of the basin used as volume for the localization.

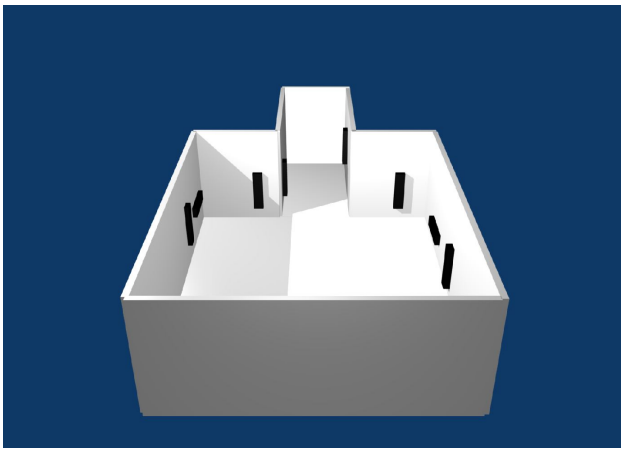

Fig. 3. Experimental setup – General layout and positions of the antenna configuration.

were configured to operate at 868 MHz, which is in accordance with European regulations for UHF RFID equipment.

In addition to an internal data processing unit the PRPS system offered a development interface to a standard PC to allow the implementation of user-designed localization algorithms. However, the data that was delivered to this interface was still preprocessed automatically by the system (including at least averaging and converting the phase differences to 16 bit values). For this work we used information about the current tag position with a precision of 1 mm (for training and testing) and the automatically determined phase differences for each of the sixteen antenna pairs.

Since we intend to replace optical navigation with our RFID navigation system, we tried to set similar working constraints for our experiments. Hence, the basin was kept empty of barriers and reflecting objects other than a robot arm connected to the CNC unit and holding the tag. In these experiments we also made no use of the special form of the basin, which can be filled with fluids emulating the absorption of a human body.

B. Experiments

We did three different experiments, creating a total of six datasets with highly differing numbers of positions and, due to technical limitations, between 20 and 30 measurements at each of these positions (see Tab. I). Each of these datasets describes a continuous space within the basin where the positions are limited to a grid with 1 mm step size because the prototype of the PRPS system monitored the tag's position only on mm-scale. The coordinate system used to represent these positions is predefined by the PRPS system and based on the coordinate system of the CNC unit.

In our first experiment we programmed the CNC unit to separately trace four linear paths in the body part of the basin. We moved the tag in x-direction in steps of 1 mm while changing y- and z-coordinates accordingly. This created the datasets L1, L2, L3 and L4 with 20 - 30 measurements at 198 positions each (see Tab. I). Every path was defined by an associated pair of antennas that marked the intersection between an extension of the path and the walls of the basin. Thus, at least one of the 16 measured phase differences was bound to be nearly optimal for the position estimation. Consequently, this experiment is considered as a first step that has to be taken for successful RFID localization. The locations of the measured paths are shown in Fig. 4.

On this basis we designed a second experiment to get closer to a three-dimensional task without adding too much complexity all at once. Again a linear path between two antennas was considered, but this time we also included an area of 10 mm $\times$ 10 mm in y-z plane around each point of the path in the dataset B1. To keep the comparability to the previous experiment, the same path as in the first dataset (L1) was traced. While this approach allows to detect slight deviations from a given path, it still guarantees distinctive phase differences for at least one pair of antennas. However, this small addition to the monitored volume already increased the amount of collected data by a factor of 100, thus making B1 consist of about 20,000 positions and 500,000 measurements (see Tab. I).

Finally, we also investigated the localization accuracy in general in a third experiment. Within the body part of the basin a dense cube was traced with 1 mm step size in all three predefined directions in space, which is shown in Fig. 5. The increase in dimensionality also gives raise to a big increase in the number of positions. Therefore, only a single dataset (C1), which covered a volume of about 3 cm $\times$ 3 cm $\times$ 3 cm, was recorded (see Tab. I).

Each of these six datasets describes a specifically selected monitored space, representing both target areas and surroundings in a real world application. Hence, these datasets were used for testing while the localization algorithm was trained on some limited subsets. Since it is impossible to calibrate a tracking system with training data from each cubic millimeter of the monitored space because of time constraints and obstacles in a real world application, a precise interpolation is of special interest for a nondeterministic localization algorithm.

To test the interpolation capabilities of our phase difference

TABLE I
CHARACTERISTICS OF THE SIX DATASETS.

Name	No. of positions	No. of measurements
L1	198	5093
L2	198	4743
L3	198	4851
L4	198	4702
B1	19890	514208
C1	34700	877393

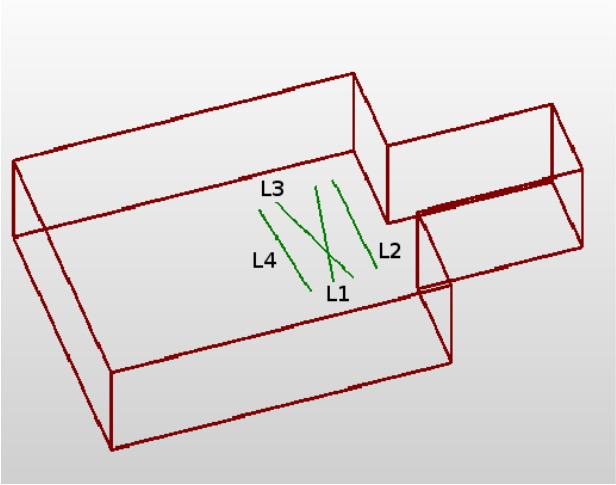

Fig. 4. Experimental setup – The path for each of the datasets L1, L2, L3 and L4 is shown.

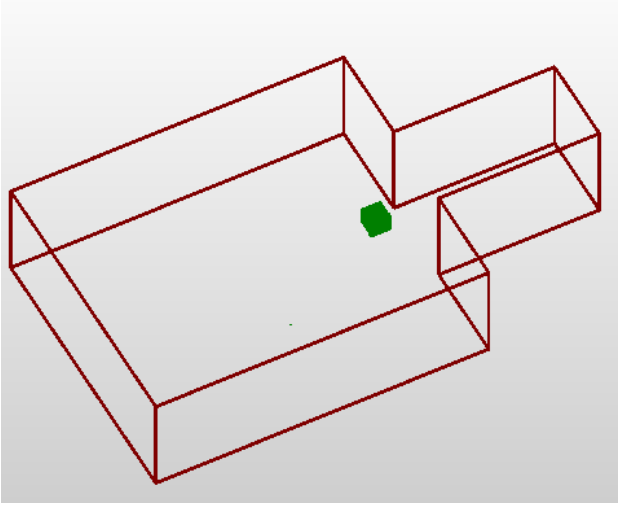

Fig. 5. Experimental setup – The data distribution of the C1 dataset is shown.

based SVR concept, we therefore created two training subsets from each dataset by applying grids with 5 mm and 10 mm step size respectively.

C. Support Vector Regression

Support vector machines (SVM) have originally been proposed as a supervised learning algorithm for binary classification [12]. In a modified formulation they can also be applied to regression tasks, which is then referred to as support vector regression (SVR) [13]. Given some data $\boldsymbol{x}_i$ and corresponding target values y_i combined to a training set $\mathcal{S} = \{(\boldsymbol{x}_1, y_1), \ldots, (\boldsymbol{x}_l, y_l)\} \subset \mathcal{X} \times \mathbb{R}$ of l examples, the SVR algorithm computes a regression function $f : \mathcal{X} \to \mathbb{R}$ given by

$$\begin{aligned} f(\boldsymbol{x}) &= k(\boldsymbol{w}, \boldsymbol{x}) + b \\ &= \sum_{i=1}^{l} \alpha_i y_i k(\boldsymbol{x}_i, \boldsymbol{x}) + b \end{aligned}$$

with optimized weights $\alpha_i \in \mathbb{R}_0^+$ for all l examples. In this equation, the Mercer kernel k is the key element for allowing nonlinear curves in $\mathcal{X}$. It implicitly maps two points from $\mathcal{X}$ to a feature space $\mathcal{F}$, where the regression is a linear problem, and computes the scalar product between them. By mapping to $\mathcal{F}$, the vector $\boldsymbol{w}$ becomes the normal vector of a hyperplane that represents points $\boldsymbol{x}_h$ that are in turn mapped to the value of the offset b by the SVR: $f(\boldsymbol{x}_h) = b$.

In the ϵ-SVR formulation the variable ϵ denotes an acceptable distance between predicted values $f(\boldsymbol{x}_i)$ and corresponding targets y_i for examples from the training set $\mathcal{S}$. To compute the weights α_i, it solves the optimization problem given by

$$\min \frac{1}{2} ||\boldsymbol{w}||^2 + C \sum_{i=1}^{l} (\xi_i + \xi_i^*)$$

$$\begin{aligned} \text{subject to :} \quad & y_i - k(\boldsymbol{w}, \boldsymbol{x}_i) - b \leq \epsilon + \xi_i \\ & y_i - k(\boldsymbol{w}, \boldsymbol{x}_i) - b \geq -\epsilon - \xi_i^* \\ & \xi_i, \xi_i^* \geq 0 \quad . \end{aligned}$$

Here C is a regularization parameter that controls the trade-off between penalizing violations of the accepted interval ϵ (denoted by ξ and ξ^*) and the complexity of the decision function $f(\boldsymbol{x})$. A solution of the convex optimization problem is usually found by means of an equivalent dual formulation. A detailed discussion of SVR can, for example, be found in the work of Vapnik [13] or Smola and Schölkopf [14].

For our experiments we used the ϵ-SVR implementation from the SHARK library [15] with radial basis function (RBF) kernels

$$k(\boldsymbol{x}_i, \boldsymbol{x}_j) = \exp\left(-\frac{||\boldsymbol{x}_i - \boldsymbol{x}_j||^2}{\sigma^2}\right) \quad .$$

The latter decision was motivated by results of Zhou and Shi for RFID localization based on RSSI vectors [11]. Regarding the choice of parameters, we found $\epsilon = 0.1$ and $\sigma = 0.01$ to produce good results in our case while the regularization parameter C was tuned by automatic model selection. This was done by a grid search to minimize the mean squared error between the estimations $f(\boldsymbol{x}_i)$ and the corresponding target values y_i on the training dataset, because for the given application a reliable estimation in a regular interval is considered more important than a potential higher overall accuracy.

IV. Experimental Results

As we discussed in section III-C, SVR maps to $\mathbb{R}$ and not $\mathbb{R}^3$. Therefore the localization was done independently in the three directions in space predefined by the CNC unit. All following references to an absolute accuracy are calculated from these three results and not direct measurements by themselves. In the following we also use the convention that a suffix 'a' indicates a training set based on the 5 mm grid and a suffix 'b' one based on the 10 mm grid.

A. Line Datasets

We began by taking measurements on four line paths between different pairs of antennas for the datasets L1 to L4. Included in these datasets are the training subsets which are denoted by the dataset name and a suffix. In the plots they are marked on the x-axis.

For the first line dataset L1 we got a mean accuracy of 4.7 ± 8.1 mm and a median of 1.6 mm if the SVR was trained on the L1a dataset, which consists of examples that are 5 mm apart of each other. If the smaller training set L1b was used, the mean accuracy increased up to 11.1 ± 14.8 mm and a median of 5.9 mm was found. The accuracy varied a lot with the tag's position for both series of measurements of the experiment, but these differences were not evenly distributed – there are many positions at which the localization error is low in contrast to just a few highly erroneous estimations. Furthermore, there's a global trend for the accuracy to get worse as the tag gets closer to one of the line's endpoints (see Fig. 6). As a consequence just the central half of the test dataset was considered as relevant while the rest was discarded for all line datasets. The result for L1 is plotted in Fig. 7 and 8. Due to this reduction the mean accuracy decreased to 1.6 ± 1.8 mm respectively 4.4 ± 4.1 mm while the median dropped to 1.0 mm for L1a and 3.3 mm in case L1b was used for training.

The results we obtained from L2 and L4 were worse than those from L1. Yet, testing on L3 proved to be remarkably successful. In the central part of this dataset, an accuracy of 0.8 ± 0.6 mm as well as a median of 0.6 mm could be reached (by training with L3a). Even with the small training set L3b, the SVR produced an estimation with an accuracy of 1.6 ± 1.5 mm. A complete list of accuracies and median values for all four line datasets is given in Tab. II.

B. Box Dataset

The box dataset B1 consists of measurements from the positions included in L1 as well as the surrounding area. In the experiments using this data we achieved a mean accuracy of 1.7 mm and 3.9 mm after training with data from a 5 mm (B1a) and a 10 mm (B1b) grid, while the median localization error was 1.3 mm and 3.0 mm, respectively (see Tab. III). Figure 9 shows the acquired accuracy in relation to the x-coordinate of the tag's position for regression based on points on a 5 mm grid. By increasing the calibration grid's step size the error interval around the actual position is raised accordingly (see Fig. 9 and 10). However, this appears to have no effect on the maximal deviations that occurred during

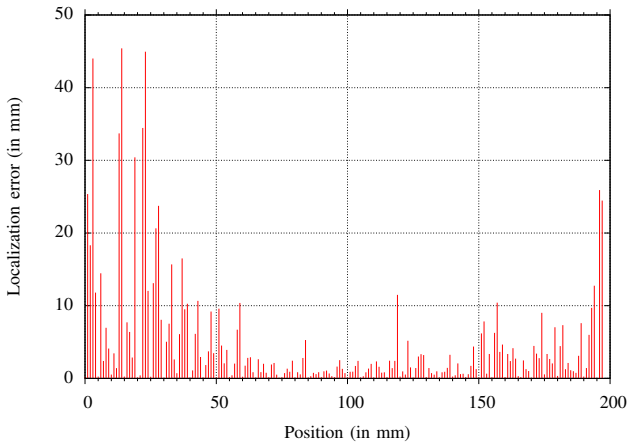

Fig. 6. Accuracy of SVR on the L1 dataset after training with L1a data. The horizontal axis shows the position of the tag relative to the CNC device's x-axis. Marks on it indicate positions used for training.

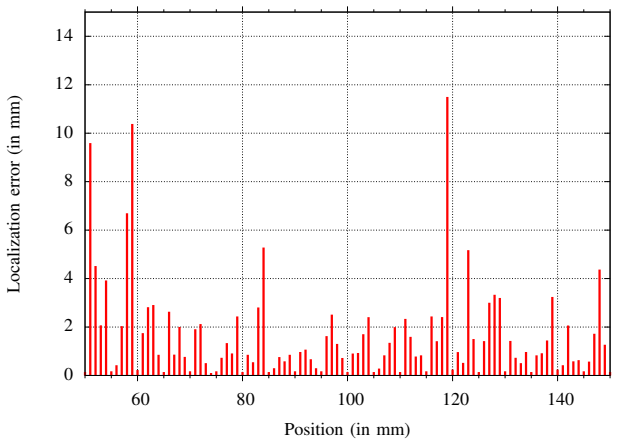

Fig. 7. Accuracy of SVR on the central part of the L1 dataset after training with L1a data. The horizontal axis shows the position of the tag relative to the CNC device's x-axis. Marks on it indicate positions used for training.

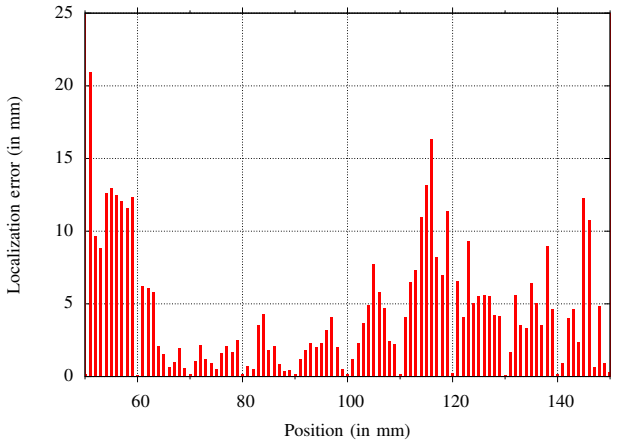

Fig. 8. Accuracy of SVR on the central part of the L1 dataset after training with L1b data. The horizontal axis shows the position of the tag relative to the CNC device's x-axis. Marks on it indicate positions used for training.

TABLE II
OVERVIEW OF THE ACCURACY OF POSITION ESTIMATION IN THE CENTRAL PART ON LINE DATASETS. ALL VALUES ARE IN MILLIMETERS.

Dataset	Test data accuracy	
	Mean	Median
L1 (L1a)	1.6±1.8	1.0
L1 (L1b)	4.4±4.1	3.3
L2 (L2a)	2.9±3.5	1.9
L2 (L2b)	6.6±5.6	5.6
L3 (L3a)	0.8±0.6	0.6
L3 (L3b)	1.6±1.5	1.1
L4 (L4a)	2.7±1.5	1.5
L4 (L4b)	4.3±4.9	2.2

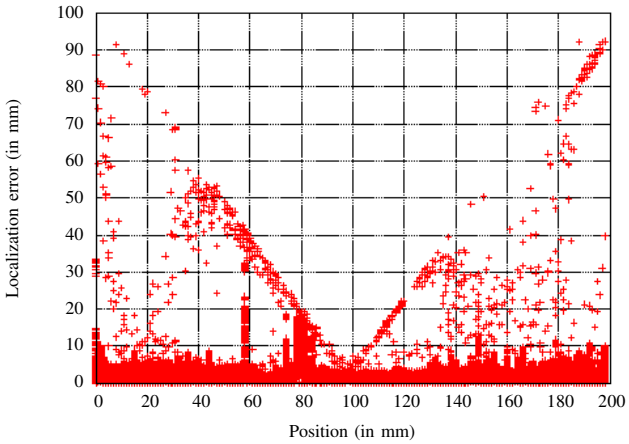

Fig. 9. Accuracy of SVR on the B1 dataset after training with B1a data. The horizontal axis indicates the position of the tag relative to the CNC device's x-axis.

TABLE III
OVERVIEW OF THE ACCURACY OF POSITION ESTIMATION ON BOX AND CUBE DATASETS. ALL VALUES ARE IN MILLIMETERS.

Dataset	Test data accuracy		Training data accuracy	
	Mean	Median	Mean	Median
B1 (B1a)	1.7±2.2	1.3	0.1±0.05	0.1
B1 (B1b)	3.9±3.4	3.0	0.1±0.05	0.1
C1 (C1a)	1.6±1.2	1.3	0.1±0.05	0.1
C1 (C1b)	7.8±5.2	6.8	0.1±0.05	0.1

the experiments. Regarding the position of measurement, we found that the central part of the box volume was still located more accurately, especially when considering the distribution along the x-axis. For the projection onto y- and z-axis this effect was less distinctive.

A cumulative distribution function (CDF) plot in Fig. 11 shows that after training on B1a most measurements result in an error between 0.6 mm and 2.0 mm. In this region the distribution scales almost linearly with the logarithm of the localization error. After using B1b, the results look mostly identical except for an increase in the corresponding error distances by a factor of 2.5.

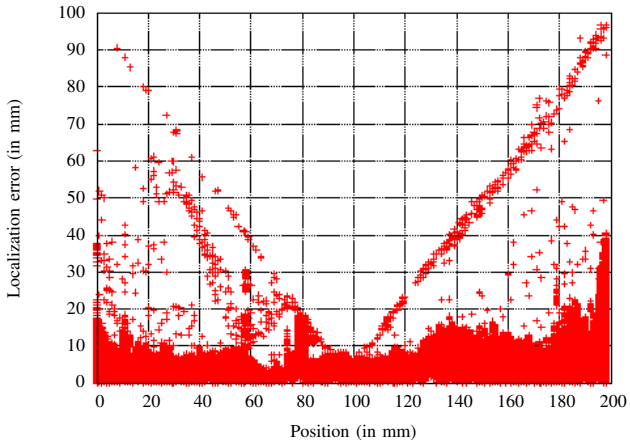

Fig. 10. Accuracy of SVR on the B1 dataset after training with B1b data. The horizontal axis indicates the position of the tag relative to the CNC device's x-axis.

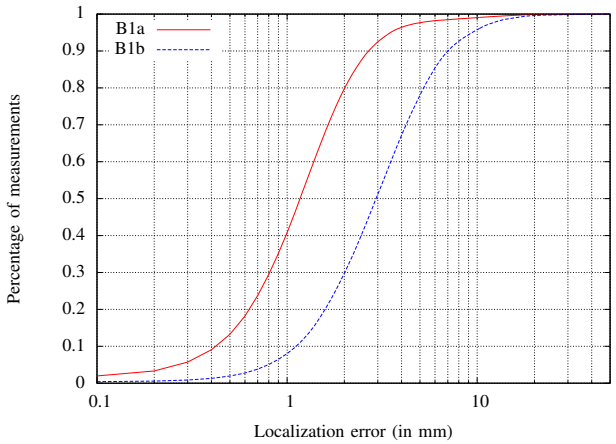

Fig. 11. Cumulative distribution function plots of the localization error of the B1 dataset. B1a denotes a training on a 5 mm grid, B1b on a 10 mm grid.

C. Cube Dataset

For the experiments on the C1 dataset a strong difference between the result on a 5 mm and a 10 mm calibration grid was observed. In the first case (C1a), a mean accuracy of 1.6 ± 1.2 mm was recorded, while it was 7.8 ± 5.2 mm for the coarse grid (C1b). In both measurements the distribution of the error values still showed a tendency to locate central positions of the cube more accurately (see Fig. 12). In contrast to the previous experiments, the point of view was of no relevance any more.

The CDF plot in Fig. 13 also shows significant differences for the two training sets. After training on C1a the distribution is almost completely identical to the one recorded for B1a in the second experiment (see Fig. 11). In contrast to that, the number of measurements with an error below a given limit after training on C1b increases much more slowly. In the latter case less than 5% of the measurements had an localization error below 1.0 mm.

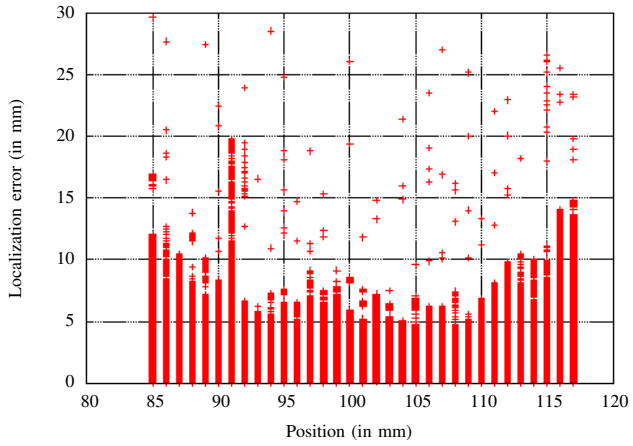

Fig. 12. Accuracy of SVR on the C1 dataset after training with C1a data. The horizontal axis indicates the position of the tag relative to the CNC device's x-axis.

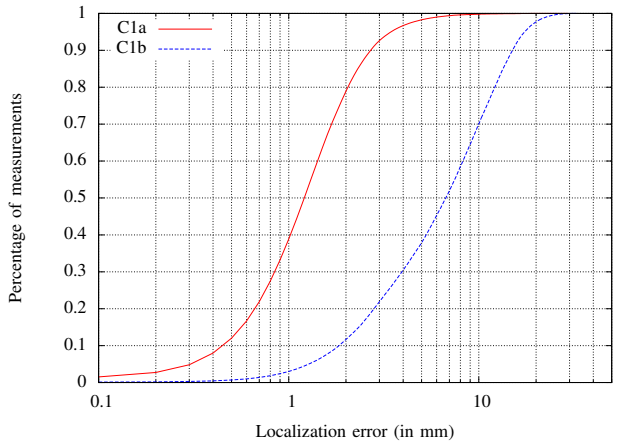

Fig. 13. Cumulative distribution function plots of the localization error of the C1 dataset. C1a denotes a training on a 5 mm grid, C1b on a 10 mm grid.

V. Discussion

In this work, we investigated the potential use of support vector regression to improve RFID localization based on multiple phase differences. This was done by performing experiments on different sets of data corresponding to localization tasks of increasing difficulty.

The simplest experiment used line datasets L1 to L4, which described a direct path between two RFID receivers. For these tests mean accuracies between 0.8 and 2.9 mm (in the central part and for training on the fine grid) were observed, while the medians were slightly lower. At least to some degree this is due to the fact, that training data was also present in the test data and is highly probable to produce localization errors way below average (see Fig. 6 and Tab. III), thus reducing the median stronger than the mean value. We also found a correlation between the distance from the line's center and the localization error. This is most likely a result from a lower number of examples located in the outer parts of the dataset, thus providing a less reliable basis for interpolation. Another more general observation is that measurements with relative high test error seem likely to be at the same positions independent of the training set. This indicates that there are detectable differences in the received signals at different locations in relation to their usability for position estimation, but further investigation into this topic is needed to determine if the effect is significant. Concerning the training process can be seen that the SVR algorithm works as intended. All positions used for training showed excellent test results with errors in the same order of magnitude as the allowed deviation parameter $\epsilon = 0.1$ mm. In addition, this accuracy doesn't seem to produce a serious overfitting as most of the test data is also located in an acceptable way.

Based on the results from L1 a second experiment was conducted. This time not only a line but also it's surroundings were traced by a tag, thus creating the box dataset B1. Although the localization task got more complex by taking into account movements in all three dimensions of space compared to the one-dimensional experiments on L1, the results for the complete dataset B1 were – at least in terms of mean accuracy – on the same level as those generated from a central part of L1. Apparently, the regression was stabilized by the additional examples in three dimensional neighborhood, reducing the percentage of border positions. As a consequence, the projections (Fig. 9 and 10) show well localized positions even in the outer parts of the box, while the worst accuracies are observed at the edges of the box. For these positions, the localization situation got indeed worse than for positions from L1, resulting in a higher maximal localization error (compare Fig. 6 and 9).

For the cube dataset C1 the situation was similar, although the tested volume was no longer in an position relative to the antennas considered ideal. However, we still got a mean accuracy of about 1.6 mm over the complete dataset, just like we did for B1. Hence, a volume of sufficient size seems to be more important for a reliable position interpolation than an optimal measurement of phase differences, which we tried to obtain in L1 to L4, although this might further increase the accuracy in some cases as seen in L3.

In general, a training with examples from a 5 mm grid proved to be much more effective than one with data from a 10 mm grid. The resulting localization deviations were reduced by more than a half if a 5 mm grid was used. For the C1 dataset, the accuracies even differed by a factor of 5. This, however, cannot be seen as representative because the cube volume offered little space for the 10 mm grid and the amount of different positions for training must be considered as very low. Furthermore, an oversized volume for training seems to be well worth the additional effort to compute the training as all experiments showed a significant stabilization of the regression in the central parts of the volume.

VI. Conclusion

Although the desired accuracy for medical applications of less than one millimeter couldn't be achieved constantly during our experiments, we still consider our results an important

step and a success for general RFID localization. We were able to reproduce the results from Hekemian-Williams et al., stating that RFID localization with an accuracy of 2 mm is possible today. In addition, there are lots of possibilities left for improving the presented method. Therefore, it is very likely that soon we will be able to reach accuracies of 1 mm and below. To begin with, the interpolation could be extended by a full model selection process, which is currently subject to an additional study. Furthermore, tracking could be introduced to limit position changes to realistic movements. And last but not least, it is still an open question whether an increase in the number of RFID receivers might further support the regression step in the localization process.

For development of real applications it is also to be investigated how changes in tag orientation and environmental variations over time will affect the localization accuracy of the presented method. Theoretically the SVR algorithm offers the possibility to include reference readings from multiple reference tags within the operating area as indicators for changes in the environment into the learning process. Tag orientation would introduce additional dimensions to the target space of the regression, which is currently not supported. However, detection of orientation is also a problem in optical tracking, which is usually solved by using a pointer with three optical markers in a known geometrical formation instead of just one marker. Such a solution is also well applicable for RFID based navigation. Yet, due to current limitations of the PRPS prototype allowing for the detection of only one tag at any given time, both problems were not considered any further in this study, but will be discussed in a later publication.

ACKNOWLEDGMENT

This work was done in cooperation with amedo smart tracking solutions GmbH. It is part of the project 'Entwicklung eines hochpräzisen Echtzeit-Ortungssystems auf RFID-Basis', which is supported by the European Union and the German 'Ministerium für Wirtschaft, Mittelstand und Energie des Landes Nordrhein-Westfalen'.

REFERENCES

[1] C. Wirtz, V. Tronnier, M. Bonsanto, S. Hassfeld, M. Knauth, and S. Kunze, "Neuronavigation. Methods and prospects," *Nervenarzt*, vol. 69, no. 12, pp. 1029–1036, 1998.

[2] Y. Enchev, "Neuronavigation: geneology, reality, and prospects," *Neurosurgical FOCUS*, vol. 27, no. 3, p. E11, 2009.

[3] J. Stiehl, W. Konermann, A. DiGioia, and R. Haaker, *Navigation and MIS in orthopedic surgery*. Springer Verlag, 2007.

[4] T. Peters, "Image-guided surgery: From x-rays to virtual reality," *Computer Methods in Biomechanics and Biomedical Engineering*, vol. 4, no. 1, pp. 27–57, 2001.

[5] J. Zhou and J. Shi, "RFID localization algorithms and applications – a review," *Journal of Intelligent Manufacturing*, vol. 20, no. 6, pp. 695–707, 2008.

[6] C. Hekimian-Williams, B. Grant, and P. Kumar, "Accurate localization of RFID tags using phase difference," in *Proceedings of the 2010 IEEE International Conference on RFID (IEEE RFID 2010)*, 2010.

[7] J. Shawe-Taylor and N. Cristianini, *Kernel Methods for Pattern Analysis*. Cambridge University Press, 2004.

[8] J. Hightower, R. Want, and G. Borriello, "SpotON: An indoor 3D location sensing technology based on RF signal strength," Department of Computer Science and Engineering, University of Washington, Tech. Rep. #2000-02-02, 2000.

[9] L. Ni, Y. Liu, Y. C. Lau, and A. Patil, "Landmarc: indoor location sensing using active rfid," in *Proceedings of the First IEEE International Conference on Pervasive Computing and Communications (PerCom 2003)*, 2003.

[10] A. Ledeczi, P. Volgyesi, J. Sallai, B. Kusy, and M. Maróti, "Towards precise indoor RF localization," in *Proceedings of the 5th Workshop on Embedded Networked Sensors (HotEmNets 08)*, 2008.

[11] J. Zhou and J. Shi, "Performance evaluation of object localization based on active radio frequency identification technology," *Computers in Industry*, vol. 60, no. 9, pp. 669–676, 2009.

[12] B. E. Boser, I. M. Guyon, and V. N. Vapnik, "A training algorithm for optimal margin classifiers," in *Proceedings of the Fifth Annual Workshop on Computational Learning Theory (COLT 1992)*. ACM, 1992.

[13] V. N. Vapnik, *The Nature of Statistical Learning Theory*. Springer Verlag, 1995.

[14] A. J. Smola and B. Schölkopf, "A tutorial on support vector regression," *Statistics and Computing*, vol. 14, no. 3, pp. 199–222, 2004.

[15] C. Igel, T. Glasmachers, and V. Heidrich-Meisner, "Shark," *Journal of Machine Learning Research*, vol. 9, pp. 993–996, 2008.